# 5. Two-layer Flows in Rotating Channels.

The exchange flow between a marginal sea or estuary and the open ocean is often approximated using two-layer stratification. Two-layer models are most valid when the interfacial region separating the upper and lower layers is relatively thin. The exchange flow in the Strait of Gibraltar exhibits this behavior, at least at certain locations and times. As shown by Figure (I10), the vertical density and velocity profiles taken near the Camerinal Sill show a relatively sharp transition between slab-like upper and lower water masses. On the other hand, the Bab al Mandab (BAM) exchange flow experiences more continuous and variations throughout the water column (Figure 5.0.1). Under such conditions, a two-layer model might still give guidance provided that motions over the water column are associated with the lowest internal mode of the stratified shear flow.

Rotational effects are often ignored in applications such as Gibraltar and the BAM, where the narrowest widths are less than or of the order of the internal Rossby radius of deformation. However valid this assumption is, it certainly fails where the strait broadens into the neighboring marginal sea or ocean.

For most deep-ocean overflows rotation is paramount but exchange dynamics are less important. However, deep overflows are often composed of fluid drawn from an intermediate water mass in the upstream basin, with a weaker contribution from deep waters. The deep and intermediate water masses may exhibit independent behavior that can be captured by treating the two as separate homogeneous layers. The flow of Antarctic Bottom Water through the Vema Channel (Figure 5.0.2) provides an example of independent behavior within the same overflowing water mass (Hogg, 1983). Upstream of the sill (right-hand section), all isopycnals slope downwards from left to right, or west-to-east as shown. However, slightly downstream of the sill section (middle frame), the slopes in the deepest (dark shaded) water are reversed and slope upwards. Isopycnals on the right-hand side of the Channel become pinched together as a result. Further downstream the deep isotherms regain their original slope (left-hand frame).

The central aim of this chapter is to explore two-layer hydraulic phenomena under the influence of rotation. However, the theory of two-layer hydraulics without rotation is quite extensive and a moderately thorough review (Sections 5.2 and 5.3) will be necessary to bring the uninitiated reader up to speed. A more extensive discussion appears in Baines (1995). Models of two-layer behavior under the influence of rotation are even more involved. Our approach will be to illustrate some of the fundamental properties of such model through the discussion of two limiting cases. In the first (Sections 5.4) the channel width is taken to be large in comparison to the internal Rossby Radius of deformation. The second limit (Section 5.5), in some respects the reverse of the first, is that of nondimensionally small potential vorticity.

## 5.1 Formulation of two-layer, semigeostrophic models.

The layout of the channel model is shown in Figure 5.1.1. The channel has a rectangular cross-section and the width and bottom elevations are denoted $w^*$ and $h^*$ as before. Two homogeneous layers of fluid are now present and we follow the oceanographic convention in numbering the top and bottom layers 1 and 2 respectively. The density $\rho_2$ of the bottom layer is only slightly greater than $\rho_1$.

In formulating the governing equations, we will employ a number of standard approximations. The first involves the treatment of the upper boundary of the two-fluid system. If this boundary were a free surface, overlain by a vacuum or by a substantially less dense fluid such as air, then free surface gravity waves would exist. In nearly all oceanographic applications the propagation speeds of these waves are much greater than the typical current velocities. In the Denmark Strait overflow, for instance, typical peak velocities are about 1m/s whereas the speeds of long, free surface gravity waves are two orders of magnitude larger. The Froude number $F_d = v^* / \sqrt{gd^*}$ based on free surface dynamics is therefore <<1. Our previous experience with homogeneous flows suggests that it is unlikely that bottom topography (or width variations) will cause significant departures of the free surface elevation from a horizontal plane. For example, equation (1.4.3) shows that the when $F_d$ is small, the departure in the free surface elevation is smaller by a factor $F_d^2$ than the variation it $w$ or $h$. For the Denmark Strait, $F_d^2$ is about $10^{-4}$. On the other hand, the speeds of the *internal* wave that propagate on the interface between the two layers are much smaller and the associated Froude numbers much larger. One might expect, then, that the typical vertical excursions of the interface will be much greater than those of the free surface. Since the latter now give a negligible contribution to variations in the upper layer depth, we simply regard the upper surface as rigid and horizontal. If $z^*=z_T^*$ denotes the elevation of this surface, $h^*$ the bottom elevation, and $d_1^*$ and $d_2^*$ the thicknesses of the two layers, then

$$z_T^* = h^* + d_2^* + d_1^*$$

The rigid lid approximation is explored more formally in Exercise 1.

We continue to assume that the fluid pressure is in hydrostatic balance. Thus the pressures in the two layers are given by

$$p_1^* = p_T^* + \rho_1 g(z_T^* - z^*) \qquad (5.1.1)$$

and

$$\begin{aligned} p_2^* &= p_T^* + \rho_1 g(z_T^* - h^* - d_2^*) + \rho_2 g(h^* + d_2^* - z^*) \\ &= p_T^* + g(\rho_2 - \rho_1)(h^* + d_2^*) + g(\rho_1 z_T^* - \rho_2 z^*) \end{aligned}, \qquad (5.1.2)$$

where $p_T^*(x^*,y^*,t^*)$ denotes the pressure at the rigid upper lid.

There are two other assumptions. The first is that the channel geometry varies only gradually along its axis, suggesting that the along-channel velocity $v_i^*$ will be geostrophically balanced. The formal arguments leading to this 'semigeostrophic' approximation are essentially those laid out in Chapter 2. The second assumption is that the density difference between the two layers is relatively small: $\Delta\rho / \bar{\rho} = (\rho_2 - \rho_1)/[\frac{1}{2}(\rho_2 + \rho_1)] << 1$. This is the basis for the Boussinesq approximation, in which the actual density $\rho_1$ or $\rho_2$ is replaced by a representative value, here the average $\bar{\rho}$, except where they are multiplied by $g$. The semigeostrophic equations governing the inviscid, Boussinesq, two-fluid system are thus:

$$fv_1{}^* = \frac{1}{\bar{\rho}}\frac{\partial p_T{}^*}{\partial x^*} \tag{5.1.3}$$

$$\frac{\partial v_1{}^*}{\partial t^*} + u_1{}^*\frac{\partial v_1{}^*}{\partial x^*} + v_1{}^*\frac{\partial v_1{}^*}{\partial y^*} + fu_1{}^* = -\frac{1}{\bar{\rho}}\frac{\partial p_T{}^*}{\partial y^*} \tag{5.1.4}$$

$$fv_2{}^* = \frac{1}{\bar{\rho}}\frac{\partial p_T{}^*}{\partial x^*} + g'\frac{\partial d_2{}^*}{\partial x^*} \tag{5.1.5}$$

$$\frac{\partial v_2{}^*}{\partial t^*} + u_2{}^*\frac{\partial v_2{}^*}{\partial x^*} + v_2{}^*\frac{\partial v_2{}^*}{\partial y^*} + fu_2{}^* = -\frac{1}{\bar{\rho}}\frac{\partial p_T{}^*}{\partial y^*} - g'\left(\frac{\partial d_2{}^*}{\partial y^*} + \frac{\partial h^*}{\partial y^*}\right) \tag{5.1.6}$$

where $g' = \Delta\rho g/\bar{\rho}$ is the reduced gravity.

The equation of mass conservation within layer $i$ is

$$\frac{\partial d_i{}^*}{\partial t^*} + \frac{\partial (u_i{}^* d_i{}^*)}{\partial x^*} + \frac{\partial (v_i{}^* d_i{}^*)}{\partial y^*} = 0 \tag{5.1.7}$$

If (5.1.5) is subtracted from (5.1.3) the result is the *thermal wind* relation for the along-channel velocity component:

$$f(v_1{}^* - v_2{}^*) = -g'\frac{\partial d_2{}^*}{\partial x^*}. \tag{5.1.8}$$

The difference in velocities between the two layers is thus proportional to the cross-channel slope of the interface.

The semigeostrophic potential vorticity within layer $i$ is defined by

$$q_i{}^* = \frac{f + \frac{\partial v_i{}^*}{\partial x^*}}{d_i{}^*}, \tag{5.1.9}$$

and conservation of this property following the fluid motion,

$$\left(\frac{\partial}{\partial t^*}+u_i^*\frac{\partial}{\partial x^*}+v_i^*\frac{\partial}{\partial y^*}\right)q_i^*=\frac{d_i^*q_i^*}{dt^*}=0\,,$$

may be shown in the same manner as for a homogeneous fluid.

In the event the potential vorticity is uniform within each layer, it is convenient to write

$$q_i^*=\frac{f}{D_{i\infty}} \tag{5.1.10}$$

where $D_{i\infty}$ represents the potential depth of layer $i$. Using this definition in (5.1.9) and combining the two results with (5.1.8) leads to an equation for the cross-channel structure of the flow

$$\frac{\partial^2 d_2^*(x^*,y^*,t^*)}{\partial x^{*2}}-L_I^{-2}d_2^*(x^*,y^*,t^*)=-\frac{f^2(z_T^*-h^*)}{g'D_{1\infty}} \tag{5.1.11}$$

where

$$L_I=\left[\frac{g'D_{1\infty}D_{2\infty}}{f^2(D_{1\infty}+D_{2\infty})}\right]^{1/2} \tag{5.1.12}$$

is the internal Rossby radius of deformation. Equation (5.1.11), which is similar to the cross-channel structure equation (2.2.2) governing the single-layer case, shows that the interface will have a boundary layer structure with $e$-folding scale $L_I$ when the channel width is >> $L_I$. Through the thermal wind relation this structure will be imposed on the shear velocity $v_1^*$-$v_2^*$. However, $v_1^*$ and $v_2^*$ need not individually decay away from the side walls.

When the flow is steady, individual transport stream functions $\psi_1^*$ and $\psi_2^*$ can be defined such that

$$v_i^*d_i^*=\frac{\partial\psi_i^*}{\partial x^*},\ \text{ and } u_i^*d_i^*=-\frac{\partial\psi_i^*}{\partial y^*} \tag{5.1.13}$$

The semigeostrophic Bernoulli functions for each layer are conserved along streamlines

$$B_1^*(\psi_1^*)=\frac{v_1^{*2}}{2}+\frac{p_T^*}{\overline{\rho}} \tag{5.1.14}$$

and

$$B_2{}^*(\psi_2{}^*) = \frac{v_2{}^{*2}}{2} + \frac{p_T{}^*}{\bar{\rho}} + g'(d_2{}^* + h^*) \qquad (5.1.15)$$

We leave it as an exercise to show

$$\frac{dB_i{}^*}{d\psi_i{}^*} = q_i{}^*. \qquad (5.1.16)$$

In most problems it is convenient to eliminate the rigid lid pressure and work with quantities that govern the internal structure of the flow. For example, subtracting (5.1.15) from (5.1.14) eliminates $p_T$*, leaving

$$\Delta B^*(\psi_1{}^*, \psi_2{}^*) = B_2{}^*(\psi_2{}^*) - B_1{}^*(\psi_1{}^*) = \frac{v_2{}^{*2} - v_1{}^{*2}}{2} + g'(d_2{}^* + h^*) \qquad (5.1.17)$$

The quantity $\Delta B^*$ is sometimes referred to as the internal energy (per unit mass).

**Exercises:**

1) Reformulate equations (5.1.3-5.1.7) allowing for a free upper surface (at which the pressure may assumed to be zero). Though inspection of these equations, formulate velocity, length and time scales based on the *internal* dynamics of the flow (i.e. use $g'$ rather than $g$). Under this scaling, show that the contribution to $d_1$* from a typical displacement of the interface is much greater than the contribution from a typical displacement of the free surface. Deduce that the free surface displacement can be neglected in the continuity equation for the upper layer, so that the upper surface can effectively be treated as rigid.

2) Show that the Bernoulli functions as defined by (5.1.14) and (5.1.15) are indeed conserved along streamlines of the respective layers, provided that the flow is steady.

3) Prove (5.1.16).

4) Using the expression for linear wave speed of an internal disturbance in a nonrotating, two layer system (see 5.2.3 of the next section) show that the two-layer Rossby radius of deformation may be interpreted as the distance that such a wave will travel in one-half rotation period.

Figure Captions

5.0.1 April 1996 CTD cast at the Bab al Mandab sill along with an month-average velocity profile for the same month. (From Pratt et al. 1999, Figure 6).

5.0.2 Three cross sections of the Vema Channel showing depths of selected potential density($\sigma$4) surfaces. Sections 1 is upstream of the sill, Section 4 is close to the sill, and Section 6 is downstream of the sill. (From Hogg, 1983).

5.1.1 Definition Sketches.

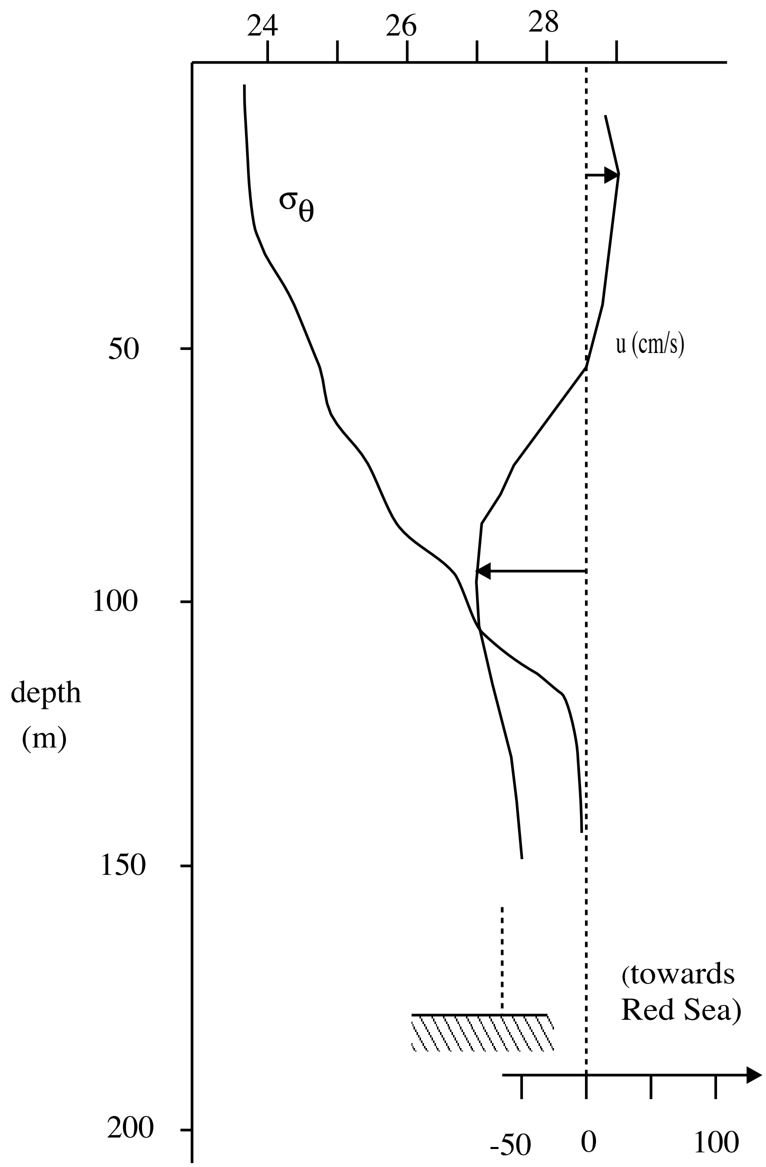


Figure 6 from Pratt et al. 1999 showing April 1996 CTD cast at BAM sill along with March 1996 ADCP monthly meanb velocity profile.

Figure 5.0.1

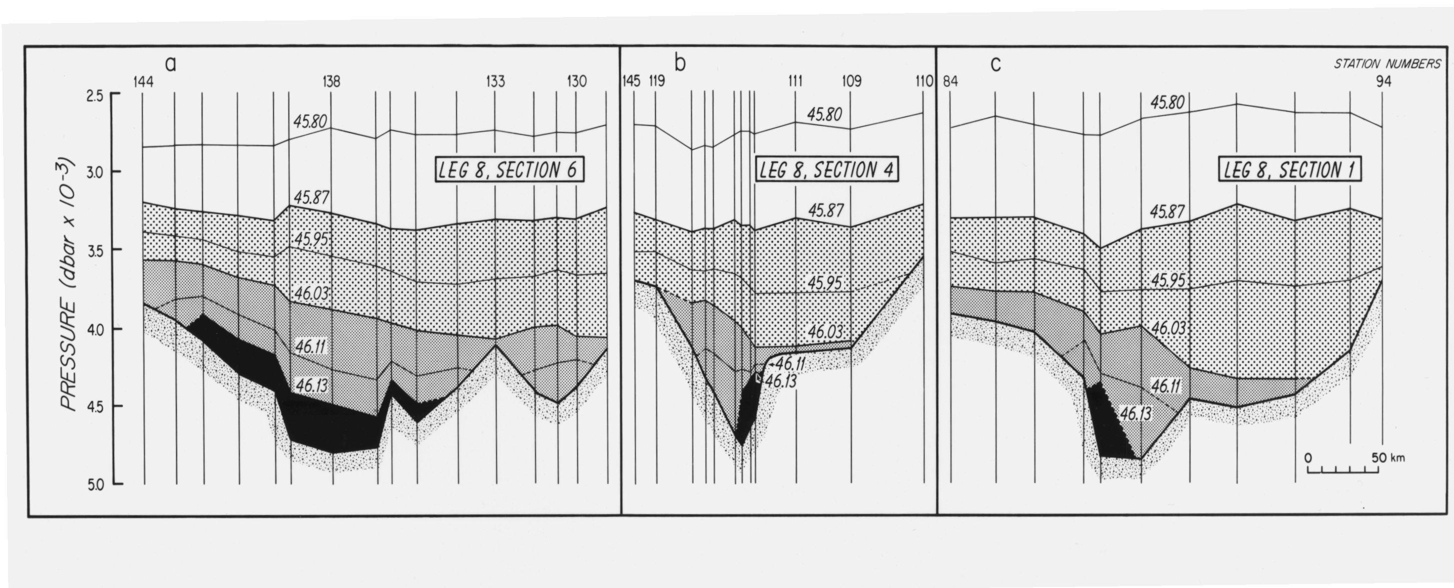


Three cross sections of the Vema Channel showing depths of selected potential density $\sigma 4$ surfaces. Sections 1 is upstream of the sill, Section 4 is close to the sill, and Section 6 is downstream of the sill.

Figure 5.0.2

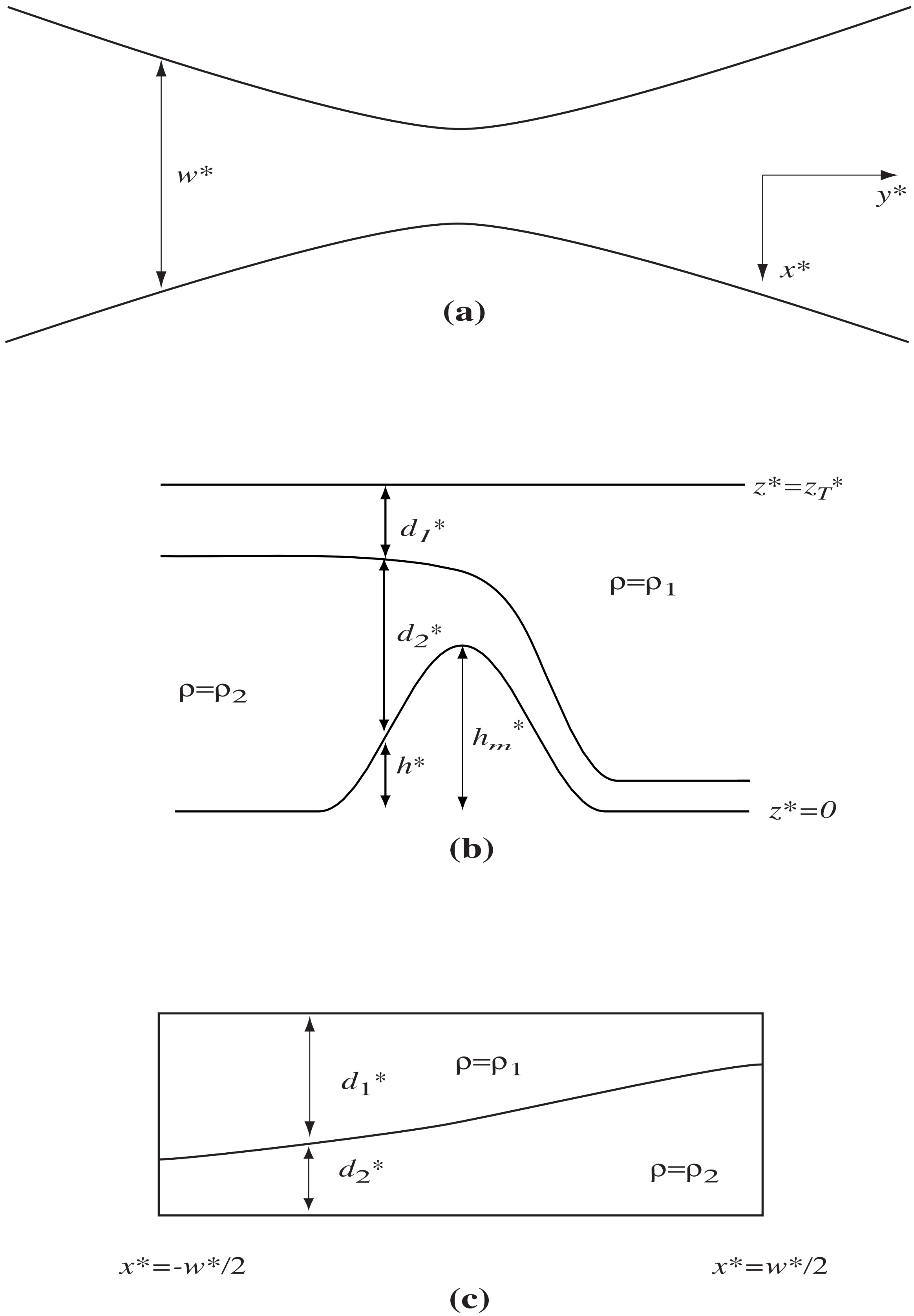
$w^*$
$y^*$
$x^*$
(a)
$z^*=z_T^*$
$d_1^*$
$\rho=\rho_1$
$d_2^*$
$\rho=\rho_2$
$h_m^*$
$h^*$
$z^*=0$
(b)
$d_1^*$
$\rho=\rho_1$
$d_2^*$
$\rho=\rho_2$
$x^*=-w^*/2$
$x^*=w^*/2$
(c)

Figure 5.1.1